

Diameters and albedos of three sub-kilometer Near Earth Objects derived from Spitzer observations

D. E. Trilling¹, M. Mueller¹, J. L. Hora², G. Fazio², T. Spahr², J. A. Stansberry¹, H. A. Smith², S. R. Chesley³, & A. K. Mainzer³

1: Steward Observatory, 933 N. Cherry Avenue, The University of Arizona, Tucson, AZ 85721; trilling@as.arizona.edu

2: Harvard-Smithsonian Center for Astrophysics, 60 Garden Street, Cambridge, MA 02138

3: Jet Propulsion Laboratory, Caltech, 4800 Oak Grove Drive, Pasadena, CA 91109

ABSTRACT

Near Earth Objects (NEOs) are fragments of remnant primitive bodies that date from the era of Solar System formation. At present, the physical properties and origins of NEOs are poorly understood. We have measured thermal emission from three NEOs — (6037) 1988 EG, 1993 GD, and 2005 GL — with Spitzer’s IRAC instrument at 3.6, 4.5, 5.8, and 8.0 μm (the last object was detected only at 5.8 and 8.0 μm). The diameters of these three objects are 400 m, 180 m, and 160 m, respectively, with uncertainties of around 20% (including both observational and systematic errors). For all three the geometric albedos are around 0.30, in agreement with previous results that most NEOs are S-class asteroids. For the two objects detected at 3.6 and 4.5 μm , diameters and albedos based only on those data agree with the values based on modeling the data in all four bands. This agreement, and the high sensitivity of IRAC, show the promise of the Spitzer Warm Mission for determining the physical parameters for a large number of NEOs.

Subject headings: minor planets, asteroids — infrared: Solar System

1. Introduction

Near Earth Objects (NEOs) are bodies whose orbits pass within a few tenths of an AU of the Earth’s orbit. As of this writing, there are around 5000 NEOs known. The Pan-STARRS

program is likely to increase the number of known NEOs to $\sim 10,000$ or more by 2013. These bodies are of critical interest to both the scientific community and the public. The NEO population is the source of potential Earth-impacting asteroids (hence a Congressional mandate to study these objects), and some may be easily reached by spacecraft, enabling our exploration of the nearby Solar System. Because NEOs have only recently been perturbed out of orbits in the main asteroid belt, and so are relatively primitive objects, they contain information that records the origin of our Solar System and that may offer insight into both the past (via delivery of organic material) and future (via impact-caused extinctions) of life on Earth. However, the physical characterization of these objects is by far outpaced by discoveries. The NEO size and albedo distributions, crucial inputs for Solar System studies as well as the assessment of the NEO Earth impact hazard, are only poorly constrained, especially at the smallest sizes (e.g., Stuart & Binzel 2004).

The diameter and albedo of asteroids can be determined from thermal-infrared observations together with appropriate thermal modeling (e.g., Lebofsky et al. 1986; Lebofsky & Spencer 1989; Harris & Lagerros 2002), provided the absolute magnitude H (optical magnitude at a standardized observing geometry; see Bowell et al. 1989) is known. A suitable thermal model for NEOs is the Near-Earth Asteroid Thermal model (NEATM, Harris 1998), which allows for simultaneous fits of the asteroid diameter, albedo, and effective surface temperature (parametrized through the beaming parameter η) (e.g., Harris 1998; Harris & Lagerros 2002).

We have measured thermal emission from three NEOs with the Spitzer Space Telescope (Werner et al. 2004) and present our data (§2) and results (§3) here. Using the NEATM, we derive albedos and diameters for all three objects (§3). In §4 we comment on the apparent thermal inertias for these objects and demonstrate that a study of NEOs could profitably be carried out with the Spitzer Warm Mission.

2. Observations and data reduction

We observed three NEOs ((6037) 1988 EG; 1993 GD; and 2005 GL) at 3.6, 4.5, 5.8, and 8.0 μm with Spitzer’s InfraRed Array Camera (IRAC; Fazio et al. 2004) using the moving cluster observing mode, tracking according to the standard NAIF ephemeris. Table 1 gives the observing log and observing geometries. These objects were chosen to be visible by Spitzer on our observing date, have small positional uncertainties, and have a range of absolute magnitudes. IRAC observes simultaneously at [3.6, 5.8] μm and at [4.5, 8.0] μm . Our dithered observations alternated between these two pairs of bandpasses to reduce the relative effects of any lightcurve variations within the observing period, and to maximize the

relative motion of the asteroid to help reject background sources. The high dynamic range mode was used, and the frame times for each object are given in Table 1.

We used the Basic Calibrated Data (v. 17.2.0) and MOPEX (v. 16.0) in the moving object mode to construct mosaics of the fields in the reference frame of the asteroid, assuming the offsets given by the NAIF ephemeris. Aperture photometry was performed using an aperture radius of 5 pixels (at 1.22 arcsec/pixel) and an annulus of 5 pixels for background measurement around the source. The aperture and annulus sizes were calibrated using one of the IRAC calibration stars (HD 165459) and the zero point set so that the measurements matched the source magnitudes given in Reach et al. (2005). 6037 and 1993 GD were detected in all four bands; 2005 GL was only detected at 5.8 and 8.0 μm (Table 1). Only 6037 is bright enough to provide good time-series photometry; no significant flux variation was detected in the ~ 15 minute span of the observations.

Due to the spectral width of the IRAC passbands, measured flux values must be color corrected. The observed asteroid fluxes comprise thermal and reflected light components, which have different color corrections (though color correction for the latter is negligible). To derive color-corrected thermal fluxes, we must first remove the reflected flux contribution in each band. The flux component from reflected sunlight was assumed to have the spectral shape of a $T = 5800$ K black body over IRAC’s spectral range. The flux level was determined from the solar flux at 3.6 μm (5.54×10^{16} mJy, Gueymard 2004), the solar magnitude of $V = -26.74$, and the asteroid’s V magnitude as determined from the observing geometry and the known H value. We assumed that asteroid reflectivity at 3.6 μm and longward is 1.4 times the reflectivity in the V band (A. Rivkin, pers. comm.), although using the naive assumption of equal reflectivity makes only a few percent difference in the resulting albedos and diameters. The estimated reflected light component was subtracted from the measured fluxes to get the (uncorrected) thermal fluxes.

Color-correction factors for the thermal flux were determined using the iterative procedure described in Mueller et al. (2007): Color-correction factors were first determined for typical NEATM parameters, the resulting fluxes were fit using the NEATM, then color-correction factors were re-derived using the best-fit NEATM parameters until convergence was reached. Color corrections and color-corrected thermal fluxes for all three targets are given in Table 2.

3. Model results and uncertainties

Thermal fluxes were measured in all four IRAC bands for (6037) 1988 EG and 1993 GD. For each target, the four-band data were fit using the NEATM by varying diameter D , albedo p_V , and η until χ^2 was minimized. D and p_V are related through the optical magnitude H : $p_V = 10^{-H/2.5} (1329 \text{ km}/D)^2$ (Fowler & Chillemi 1992). (In all cases we assume emissivity of 0.9 and standard scattering behavior in the visible, resulting in a phase integral of 0.39.) These best-fit (floating η) values for D , p_V , and η are given in Table 2 and the corresponding model spectra are shown in Figure 1.

For these four-band (floating η) fits, we use a Monte Carlo analysis to estimate the statistical uncertainty of our results. 300 random sets of flux values were generated such that their mean and standard deviation match the measured fluxes and flux uncertainties, respectively. Each trial was fit using the NEATM as above. The standard deviations of the resulting diameter and albedo values were taken to be the statistical uncertainties on our four-band results (Table 2). We do the same NEATM/Monte Carlo analysis using just the 5.8 and 8.0 μm data for the brighter two objects (Table 2), allowing us to assess systematic variations in model results. However, because the measurements of 2005 GL have relatively low significance, this Monte Carlo approach does not work, and we require a proxy technique to determine variations among models, as follows.

With this Monte Carlo proxy model, the nominal fit is determined in the usual way (NEATM, as above). We then use the NEATM to fit a “hot” solution, where the short wavelength data is increased by 0.7σ and the long wavelength solution is decreased by 0.7σ relative to the nominal flux values (σ is the measurement error). We also fit a “cold” solution, which has short band decreased and the long band increased by 0.7σ . The range in derived albedo and diameter then is derived from the range of values produced by the hot and cold solutions. We show in Table 2 that for 6037 this hot/cold proxy approach replicates the full Monte Carlo result quite closely. We present this proxy model here because, in general, this approach is a useful substitute for full Monte Carlo modeling. However, for 2005 GL, the significance of our measurements is so poor that even this technique does not work (producing implausible albedos around 2 and unlikely η values around 0.38). We must therefore move to yet a simpler technique to assess systematic errors due to model variations.

Delbo’ et al. (2003, 2007); Wolters et al. (2008) derived an empirical relationship between the phase angle α at which observations are made and the best-fit η . This “fixed η ” technique works here because the number of free parameters is decreased by one: the surface temperature is fixed due to the fixed η (compare to the hot/cold models above). Thus, we produce “fixed η from α ” solutions for 2005 GL, as well as for 6037 (fitting 5.8 and 8.0 μm data and fitting 3.6 and 4.5 μm data) and for 1993 GD (with the same data subsets)

(Table 2). In the interest of assessing variations due to different model solutions, we also derive “fixed η from α ” solutions for 2005 GL using just 5.8 μm data and using just 8.0 μm data (Table 2). The formal errors on these fixed η solutions are derived directly from the measurement errors: because any acceptable fit must pass within the measurement error bars, the percent error on diameter is equal to the percent error on the best measurement utilized in the fit, divided by two (since flux is proportional to diameter squared). The albedo uncertainty is twice that of the diameter uncertainty, or equal to the uncertainty on the best measurement utilized.

We take our final model solutions to be the averages of the solutions from the various techniques (Table 2). This allows us to capture the scatter among the different model solutions in the error bars on our final solutions. The uncertainties on diameter are around 7% for the strongly detected 6037 and around 16% for the less well detected 1993 GD. For 2005 GL, where there are only three models, all of the same type, the uncertainty on diameter is also around 16%. Uncertainties on albedo are twice those on diameter. These final solutions are given in Table 2 and plotted in Figure 1.

Our diameter solutions are hindered by our lack of knowledge about physical target properties such as shape, spin state, thermal inertia, and surface roughness, all of which affect surface temperatures and hence thermal flux; together, these typically imply an uncertainty around 15% (e.g., Wright 2007), comparable to the systematic errors we estimate from our cross-model comparisons above. More realistic thermophysical modeling (e.g., Harris & Lagerros 2002) would require models for shape and spin state as inputs, but those are unlikely to become available for our targets in the near future.

Additional diameter uncertainty derives from the rotational flux variability (lightcurves) of our targets. The peak-to-peak lightcurve amplitude of 6037 is¹ around 0.2 mag. Following the arguments presented in Appendix A, we find that the resulting diameter uncertainty due to lightcurve effects is negligible: less than 4%. Nothing is known about the lightcurves of our remaining targets. Given their small size, their lightcurves are likely to have a rather large amplitude and small period (Pravec et al. 2002). By virtue of our observation design, measured fluxes in all four channels are effectively averaged over ~ 900 s (1993 GD) and $\sim 2,000$ s (2005 GL). Assuming a lightcurve amplitude of 1 mag and a period of 1 hour for 2005 GL, the corresponding diameter uncertainty due to lightcurve effects would be around 2% – negligibly small.

The final diameter uncertainties are therefore the combination of uncertainties from modeling ($<20\%$); uncertainties in physical properties (15%); and lightcurve effects (small).

¹<http://www.asu.cas.cz/~ppravec/neo.html>

The total uncertainties on diameters are likely to be around 20%, including errors from both measurement and systematic uncertainties.

The corresponding albedo uncertainty due to scatter in model results and ignorance of physical properties is therefore around 40%. Uncertainties in H , which leave the best-fit diameter estimate practically unchanged (Harris & Harris 1997), add to the error budget for p_V . This effect is small for 6037 (where the uncertainty in H is estimated to be 0.15 mag), but H could be in error by 0.3 mag or more for the other two targets, leading to errors in p_V of 30% or more. Combining these two uncertainties (40% from above and 30% from H uncertainty), we therefore estimate the total uncertainty on our albedo determinations to be around 50%.

4. Discussion

All three objects have diameters less than 500 meters, making them among the smallest NEOs with known albedos and diameters, and among the smallest individual objects studied with the Spitzer Space Telescope. All three objects also have albedos close to 0.3, in agreement with the idea that the NEO population is dominated by S-class asteroids (e.g., Binzel et al. 2004). Binzel et al. (2004) also found that the albedos for S-class (and related classes) NEOs rise from their main belt average value around 0.22 to greater than 0.3 for objects $\lesssim 500$ m. Our results appear to confirm this trend (Figure 1), though with small numbers and not insignificant error bars. It is quite premature to discuss the reality of the potentially interesting downward turn at even smaller sizes.

The best-fit (floating) η values found for 6037 and 1993 GD are roughly consistent with empirical expectations (Delbo’ et al. 2003), which were recently used by Delbo’ et al. (2007) to determine the typical thermal inertia of $D \sim 1$ km NEAs. Thermal inertia is indicative of the presence or absence of loose material (regolith) on the surface and is a key parameter for model calculations of the Yarkovsky effect, a non-gravitational force that severely influences the orbital dynamics of small asteroids. (Note that Vokrouhlický et al. (2005) list 6037 as a potential target for direct observations of the Yarkovsky effect.) Our results suggest that our targets have unremarkable thermal inertias and may be similar to the 320 meter diameter S-type NEO (25143) Itokawa (Müller et al. 2005; Mueller 2007), the target of the Hayabusa mission. However, more work and a systematic, large survey are needed to determine the typical thermal inertia of sub-km NEAs.

For 6037 and 1993 GD the diameters and albedos we derive using only 3.6 and 4.5 μm data are in agreement with our other model solutions, particularly for 6037, which is strongly

detected (SNR>10) in both bands. This agreement has important implications for the Spitzer Warm Mission. After Spitzer’s onboard cryogen is exhausted, observations in IRAC bands 1 and 2 (3.6 and 4.5 μm) can still be made with essentially no loss of sensitivity. Our results show the promise of capitalizing on the superior sensitivity of IRAC to determine the physical properties of a large number of NEOS during the Spitzer Warm Mission.

We thank the referee for a number of useful suggestions. We thank Tom Soifer for allocating Director’s Discretionary time for this project and Mike Werner for helpful suggestions. We acknowledge the extremely rapid release of these data by the SSC and Sean Carey for MOPEX advice. Andy Rivkin helped us estimate the relative spectral reflectances of asteroids and Rick Binzel provided us his data that we plotted in Figure 1. This work is based on observations made with the Spitzer Space Telescope, which is operated by JPL/Caltech under a contract with NASA. Support for this work was provided by NASA through an award issued by JPL/Caltech.

Facilities: Spitzer(IRAC)

A. The effect of unknown lightcurve variations on diameter uncertainties

Uncertainties in diameter can arise from the rotational flux variability (lightcurve) of an observed asteroid. To first order, the projected area A of an asteroid with a double-peaked lightcurve varies as $A(\phi)/A_0 = 1 + (10^{\frac{\Delta m}{2.5}} - 1) \sin 2\phi$, where ϕ is rotational phase, A_0 is the average area, and Δm is the peak-to-peak lightcurve amplitude. For an instantaneous area measurement at a random time, the expectation value is A_0 and the standard deviation is $\sigma_A = A_0(10^{\Delta m/5} - 1)/\sqrt{2}$. Since area is proportional to diameter squared, the lightcurve-induced contribution to the fractional diameter uncertainty is $\sigma_D = (10^{\Delta m/5} - 1)/\sqrt{8}$. Therefore, for objects whose lightcurve amplitudes but not periods are known, σ_D can be estimated. Only for objects with $\Delta m \geq 1.9$, which is a very large amplitude lightcurve, is σ_D greater than 50%.

Some observations may span a significant portion of an asteroid’s rotation period; our relatively long integrations on 1993 GD and 2005 GL may be examples. The time-averaged lightcurve-induced diameter uncertainty is $\sigma_D \langle t \rangle = \sigma_D \times S$, where S is a smoothing factor and is equal to $|\sin \phi|/\phi$, with $\phi = 2\pi T/P$ (the rotational phase, as above); T giving the duration of the measurement; and P being the rotation period.

For all $T \gtrsim 0.4 P$, it is the case that $S \lesssim 0.2$, so $\sigma_D \langle t \rangle$ will almost always be small for sufficiently long observations. In cases where an asteroid’s lightcurve period is known, an

observing plan that results in small σ_D can be created without requiring that the thermal and reflected light observations be simultaneous or even phased. Finally, we conclude that for very small asteroids, uncertainties introduced by lightcurve effects will almost always be small, as follows. Some very small asteroids have very short rotation periods (just a few minutes), and most generally will require long integration times. Therefore, T is likely to be $\gtrsim 0.4 P$, making $\sigma_D \langle t \rangle$ small.

REFERENCES

- Binzel, R.P., Rivkin, A.S., Stuart, J.S., Harris, A.W., Bus, S.J., & Burbine, T.H. 2004, *Icarus*, 170, 259
- Bowell, E., Hapke, B., Domingue, D., Lumme, K., Peltoniemi, J., & Harris, A.W. 1989, in *Asteroids II*, eds. R.P. Binzel et al. (Tucson: Univ. of Arizona Press), 524
- Delbo', M., Harris, A.W., Binzel, R.P., Pravec, P., Davies, J.K., 2003, *Icarus*, 166, 116
- Delbo', M., dell'Oro, A., Harris, A.W., Mottola, S., Mueller, M. 2007, *Icarus*, 190, 236
- Fazio, G. G., et al. 2004, *ApJS*, 154, 10
- Fowler, J.W. & Chillemi, J.R. 1992, in *The IRAS Minor Planet Survey*, ed. E.D. Tedesco (Hanscom Air Force Base, Massachusetts), 17
- Gueymard, C.A. 2004, *Solar Energy*, 76, 423
- Harris, A.W. 1998, *Icarus*, 131, 291
- Harris, A.W. & Harris, A.W. 1997, *Icarus*, 126, 450
- Harris, A.W. & Lagerros, J.S.V. 2002, in *Asteroids III*, eds. W.F. Bottke et al. (Tucson: Univ. of Arizona Press), 205
- Lebofsky, L.A. et al. 1986, *Icarus*, 68, 239
- Lebofsky, L.A. & Spencer, J.R. 1989, in *Asteroids II*, eds. R.P. Binzel et al. (Tucson: Univ. of Arizona Press), 128
- Mueller, M. 2007, Ph.D. thesis, Freie Universitaet Berlin, Germany (<http://www.diss.fu-berlin.de/2007/471/indexe.html>)
- Mueller, M., Harris, A.W., & Fitzsimmons, A. 2007, *Icarus*, 187, 611

- Müller, T.G., Sekiguchi, T., Kaasalainen, M., Abe, M., & Hasegawa, S. 2005, *A&A*, 443, 347
- Pravec, P., Harris, A.W., & Michałowski, T. 2002, in *Asteroids III*, eds. W.F. Bottke et al. (Tucson: Univ. of Arizona Press), 113
- Reach, W. T. et al. 2005, *PASP*, 117, 978
- Stuart, J.S. & Binzel, R.P. 2004, *Icarus*, 170, 295
- Vokrouhlický, D., Čapek, D., Chesley, S.R., & Ostro, S.J. 2005, *Icarus*, 173, 166
- Werner, M. et al. 2004, *ApJS*, 154, 1
- Wolters, S.D., Green, S.F., McBride, N., & Davies, J.K. 2008, *Icarus*, 193, 535
- Wright, E.L. 2007, preprint (astro-ph/0703085)

Table 1. Observing log

Target	AOR	UT Date	H (mag)	r (AU)	Δ (AU)	α (deg)	t_{frame} (sec)	t_{exp} (sec)	$F_{3.6}$ (μJy)	$F_{4.5}$ (μJy)	$F_{5.8}$ (μJy)	$F_{8.0}$ (μJy)	Comment
(6037) 1988 EG	26984704	2008-Apr-07 21:34	18.7	1.24	0.42	46.96	12	120	50 (4)	180 (7)	856 (24)	3013 (34)	1
1993 GD	26985216	2008-Apr-07 21:57	20.8	1.28	0.49	46.64	30	450	11 (3)	36 (3)	124 (13)	436 (13)	2
2005 GL	26984960	2008-Apr-07 18:35	21.2	1.37	0.71	44.06	100	1000	52 (7)	108 (7)	3

Note. — We list here the AOR (unique observation ID; these observations were made as part of PID 476); midtimes of the observations; the Solar System absolute magnitude H , from the MPC; the target heliocentric distance r , Spitzer-centric distance Δ , and phase angle α at time of observation; the individual frame time; the total exposure time; and the measured (not color-corrected) fluxes in the four IRAC bandpasses, with the errors in parentheses. The effective wavelengths of these four bandpasses are [3.550, 4.493, 5.731, 7.872] μm . The errors listed here do not include the 3% absolute calibration uncertainty (Reach et al. 2005). It is difficult to estimate upper limit fluxes at 3.6 and 4.5 μm for 2005 GL due to many faint star trails at the position of the asteroid. Notes: (1) H magnitude uncertainty around 0.15; this object has a known lightcurve with period near just under 3 hours and amplitude 0.2 mag. (2) H magnitude uncertainty around 0.4. (3) H magnitude uncertainty around 0.3.

Table 2. Physical properties of NEOs

Target	Thermal fluxes (μJy)				diameter (m)	albedo	η	Model
	3.6 μm	4.5 μm	5.8 μm	8.0 μm				
(6037) 1988 EG	10	142	806	2970	435 (23)	0.31 (0.03)	1.64 (0.11)	Floating η
	806	2970	374 (34)	0.43 (0.08)	1.30 (0.18)	Floating η
	806	2970	372 (35)	0.42 (0.07)	1.29 (0.17)	Floating η , hot/cold MC proxy
	806	2970	414 (4)	0.34 (0.006)	1.52	Fixed η from α
	10	142	398 (15)	0.37 (0.03)	1.52	Fixed η from α
	399 (27)	0.37 (0.05)	1.45 (0.15)	Average of model results
1993 GD	6	31	117	430	143 (11)	0.42 (0.07)	1.02 (0.12)	Floating η
	117	430	170 (31)	0.32 (0.12)	1.34 (0.36)	Floating η
	117	430	184 (6)	0.25 (0.02)	1.52	Fixed η from α
	6	31	213 (17)	0.19 (0.03)	1.52	Fixed η from α
	178 (29)	0.30 (0.10)	1.35 (0.24)	Average of model results
2005 GL	49	107	147 (10)	0.27 (0.03)	1.48	Fixed η from α
	107	145 (6)	0.29 (0.02)	1.48	Fixed η from α
	49	...	191 (12)	0.17 (0.03)	1.48	Fixed η from α
	161 (26)	0.24 (0.06)	1.48	Average of model results

Note. — We list here the color-corrected thermal fluxes (reflected light components subtracted) for each target. Errors (omitted for clarity) on these thermal fluxes are equal to the measurement errors given in Table 1 divided by our derived color corrections of [1.16, 1.09, 1.04, 1.01] for [3.6, 4.5, 5.8, 8.0] μm . (The same color corrections apply for all three targets. We neglect uncertainties in

reflected light flux, that is, we assume that those uncertainties are zero). We list solutions (with errors in parentheses) to four-band and two-band sets of data, indicating in the flux columns which measurements are being used. A range of models, discussed in the text, are presented, as well as the average results from the various models. The average results are also plotted in Figure 1.

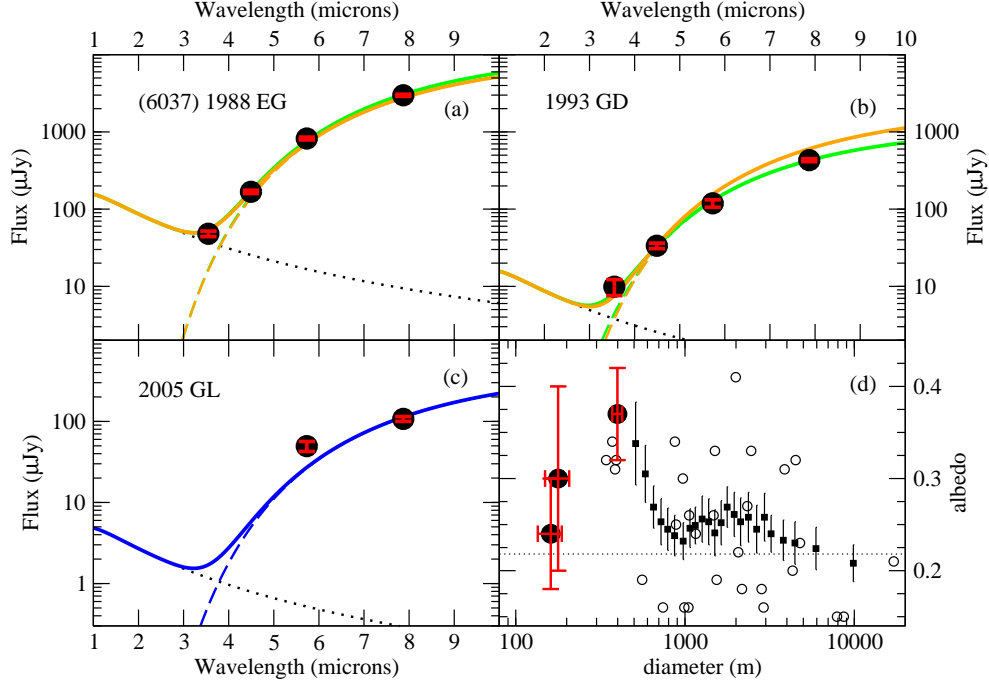


Fig. 1.— *Panels a,b,c*: Spectral energy distributions for the three observed NEOs. Data points (black filled symbols with red error bars overplotted) show our color-corrected total (reflected plus thermal) fluxes. Green curves (panels a,b) show fits to four band data. Orange curves (panels a,b) show fits to data at 3.6 and 4.5 μm only, with η fixed. Blue curves (panel c) show fits to data at 5.8 and 8.0 μm only, with η fixed. Dashed lines indicate thermal components and dotted lines indicate reflected light components of the total flux, which is plotted with solid lines. In panels (a) and (b) the orange curves lie nearly on top of the green curves, implying that the two fits are very similar (but making the green curves difficult to see). *Panel d*: A modified version of Figure 8 from Binzel et al. (2004) that also plots the average diameters and albedos that we report here as large black circles with red error bars; see Table 2. The open small black circles are individual data points and filled black squares are mean values for S-class (and related classes) NEOs (Binzel et al. 2004). The dotted line is the mean albedo for main belt S class asteroids. The error bars on the solutions here reflect the scatter in the model solutions, but do not include additional uncertainties that may derive from ignorance of physical properties of the asteroids or uncertainties in H (see text for discussion).